

# Fully packed quantum loop model on the square lattice: Phase diagram and application for Rydberg atoms

Xiaoxue Ran,<sup>1</sup> Zheng Yan,<sup>1,2,\*</sup> Yan-Cheng Wang,<sup>3</sup> Junchen Rong,<sup>4</sup> Yang Qi,<sup>2,5,6</sup> and Zi Yang Meng<sup>1,†</sup>

<sup>1</sup>*Department of Physics and HKU-UCAS Joint Institute of Theoretical and Computational Physics,  
The University of Hong Kong, Pokfulam Road, Hong Kong SAR, China*

<sup>2</sup>*State Key Laboratory of Surface Physics, Fudan University, Shanghai 200433, China*

<sup>3</sup>*Beihang Hangzhou Innovation Institute Yuhang, Hangzhou 310023, China*

<sup>4</sup>*Institut des Hautes Études Scientifiques, 91440 Bures-sur-Yvette, France*

<sup>5</sup>*Center for Field Theory and Particle Physics, Department of Physics, Fudan University, Shanghai 200433, China*

<sup>6</sup>*Collaborative Innovation Center of Advanced Microstructures, Nanjing 210093, China*

(Dated: December 27, 2022)

The quantum dimer and loop models attract great attentions, partially because the fundamental importance in the novel phases and phase transitions emerging in these prototypical constrained systems; and partially due to their intimate relevance towards the on-going experiments on Rydberg atom arrays in which the blockade mechanism naturally enforces the local constraint. Here we show, by means of the sweeping cluster quantum Monte Carlo method, the complete ground state phase diagram of the fully packed quantum loop model on the square lattice. We find between the lattice nematic (LN) phase with strong dimer attraction and the staggered phase (SP) with strong dimer repulsion, there emerges a resonating plaquette (RP) phase with off-diagonal translational symmetry breaking. Such a novel phase is separated from the LN via a first order transition and from the SP by the famous Rokhsar-Kivelson point. Our renormalization group analysis reveals the different flow directions, fully consistent with the order parameter histogram in Monte Carlo simulations. The realization and implication of our phase diagram in Rydberg experiments are proposed.

*Introduction.*— Quantum dimer and loop models and their classical cousins are the prototypical constrained many-body systems [1–17]. In 2d lattices, the quantum dimer model (QDM) usually refers to the local constraint with dimer covering of one dimer per site and the quantum loop model (QLM) two dimers per site. The QDM and QLM can be viewed as the incarnation of the resonating valence bond wavefunctions [5, 18, 19] and the low-energy effective model of frustrated magnets [10–12], and they offer the clear realization of the lattice gauge theory and conformal quantum criticalities [17, 20–26]. In recent years, these constrained quantum many-body models arouse broad research interests since they can be realized in the Rydberg atom arrays trapped in optical tweezers [27–29], in which each dimer is identified with an atom excited to a Rydberg state by laser pumping [30–32]. The observations of quantum phase transitions and the signature of topological orders from such experiments [33–36] have posted the questions of the complete and precise theoretical understanding of the phase diagrams of QDM and QLM to the community.

However, the question is by no means easy to answer. The precise computation of the physical properties of QDM and QLM are difficult besides few limits such as the Rokhsar-Kivelson (RK) point [5, 37, 38] or exact diagonalization and DMRG for small clusters and Green Function Monte Carlo simulations at intermediate system sizes [23–26, 39–41], and it is only recent, thanks to the invention of the sweeping cluster quantum Monte Carlo (QMC) method [32, 42–44] which solves these constrained models in the path-integral via efficient Monte Carlo update scheme respecting the local constraints, the

ground state phase diagrams and the low-energy excitations therein of QDM on the square [15, 32, 45, 46], triangular [43] and of QLM on triangular lattices [47] have been obtained with controlled finite size analysis towards the thermodynamic limit (TDL). Meanwhile, the phase diagrams of the QDM and QLM on other 2d lattices, as simple as QLM on square lattice, are still largely absent and their implications to the on-going experiments in Rydberg arrays are yet to be explored.

Here, we answer the question of the phase diagram of the QLM on the 2d square lattice with the sweeping cluster QMC. Via the finite size scaling towards the TDL and the renormalization group analysis of the effective height field action [5, 7], we find there exist a lattice nematic (LN) phase with strong dimer attraction and a staggered phase (SP) with strong dimer repulsion, and in between, there further emerges a resonating plaquette (RP) phase with off-diagonal long-range order that breaks the lattice translational symmetry. Such a novel phase is separated from the LN via a first order transition and from the SP by the RK point. This intermediate RP phase, diagnosed not by the dimer correlation but by the off-diagonal  $t$ -term (see the Hamiltonian Eq. (1)) correlation, has both theoretical interests with its dangerously irrelevant  $\cos(4\pi h)$  operator at the RK point similar as the second length scale in the deconfined quantum criticality [48, 49], and more importantly, the experimental detectable signature in the Rydberg atom arrays on checkerboard lattice. Our results therefore respond to the urgent question from the fast progress in experiments and can be used to guide future ones.

*Model and methods.*— The Hamiltonian of QLM on a

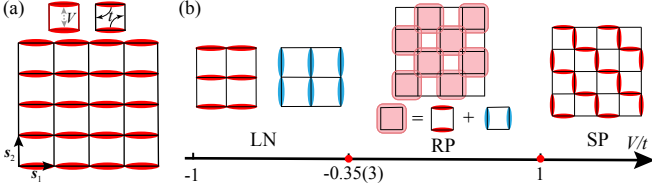


FIG. 1. **Fully packed quantum loop model on the square lattice.** (a) Schematic representation of the QLM;  $\mathbf{s}_1$  and  $\mathbf{s}_2$  are the primitive vectors. The  $t$ - and  $V$ -terms in the Hamiltonian Eq. (1) are depicted in the upper inset. The dimer configuration sketched is one of the two LN patterns, with fully packed loops along the  $\mathbf{s}_1$  direction. (b) Phase diagram of the QLM obtained from our simulations. The left subfigure illustrates the two LN dimer configurations. The first row of the middle subfigure is one of the two resonating plaquette (RP) patterns and the second row is the resonating dimer pair within one plaquette. The first-order phase transition between the LN and RP states occurs at  $V = -0.35(3)$ . The right subfigure shows one representative staggered phase (SP) state with  $V > 1$ . The SP states have extensive ground state degeneracy  $\sim 4 \times 2^p$  ( $p \propto L$  as discussed in Ref. [39]).

square lattice is defined as

$$H = -t \sum_{\text{plaq}} (|\square\rangle\langle\square| + h.c.) + V \sum_{\text{plaq}} (|\square\rangle\langle\square| + |\blacksquare\rangle\langle\blacksquare|), \quad (1)$$

where the summation covers all plaquettes and as shown in Fig. 1 (a), the local constraint is implemented such that there must be two dimers touching every lattice site in every dimer configuration. The kinetic term –  $t$ -term – changes the dimer covering of flippable plaquettes, and the potential term –  $V$ -term – is repulsive ( $V > 0$ ) or attractive ( $V < 0$ ) between dimers facing each other on a plaquette, and we also allow the configurations with three dimers on a plaquette. The RK point is located at  $V/t = 1$  and described by an emergent  $U(1)$  symmetry in the effective height model description [5, 7] (see below). We set  $t = 1$  as the unit of energy in our simulations.

We employ the sweeping cluster QMC [32, 42–44] to solve the model and extrapolate finite size results to the TDL. Our simulations are performed on the square lattice with periodic boundary condition and system sizes  $N = L^2$  with  $L = 8, 12, 16, 20, 24$  and  $28$ , while setting the the inverse temperature  $\beta = 2L$ . Detailed description of the QMC implementation can be found in the Supplementary Material (SM) [50].

*Phase diagram and transitions.*—To explore the phase diagram of the Hamiltonian in Eq. (1), we first use three order parameters given by  $\phi_1 = \frac{1}{N}|N_{\blacksquare}^c - N_{\blacksquare}^c|$ ,  $\phi_2 = \frac{1}{N}|N_{\blacksquare}^c - N_{\blacksquare}^c|$  and  $\phi_3 = \frac{1}{N}|N_{\blacksquare}^c - N_{\blacksquare}^c|$ , where  $N^c$  is the number of a specific dimer pattern (including  $\blacksquare$ ,  $\blacksquare$ ,  $\blacksquare$ ,  $\blacksquare$ ,  $\blacksquare$  and  $\blacksquare$ ) on all plaquette of the dimer covering  $c$ .  $\phi_1$  and  $\phi_2$  are the single- and dimer-pair rotational symmetry breaking order parameters, respectively.

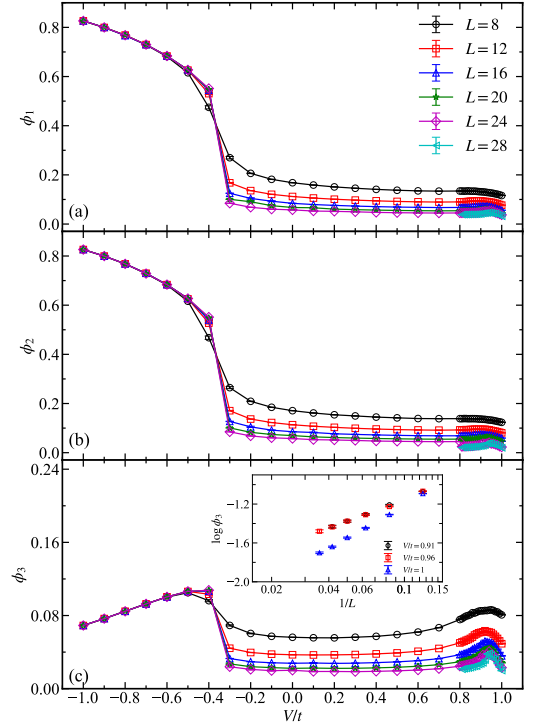


FIG. 2. **Quantum phase transitions in the square lattice QLM.** (a), (b), and (c) are the dimer order parameters  $\phi_1, \phi_2$ , and  $\phi_3$  as a function of  $V$ . The LN–RP first-order transition occurs at  $V = -0.35(3)$ . The inset of (c) shows the instability of the rotational symmetry breaking inside each plaquette close to the RK point, is a finite size effect and in a log-log plot,  $\phi_3$  at  $V \sim 0.9$  goes to zero in a power-law with  $L$ .

As shown in Fig. 1 (b), both of them can be used to detect the LN phase where the global lattice rotation symmetry is broken, and  $\phi_3$  can be used to further detect whether in each plaquette, there is a further local rotational symmetry breaking (as show in Fig. 2 (b) and explained below,  $\phi_3$  is not the order parameter of RP phase but nevertheless helps to find an irrelevant  $\mathbb{Z}_4$  instability therein close to the RK point).

Our data in Fig. 2 (a), (b) and (c) reveal  $\phi_1, \phi_2$  and  $\phi_3$  detect the LN–RP first order phase transition at  $V = -0.35(3)$  (and we further show a coexistence of both phases in the histogram at  $V = -0.36$  in Fig. 4 (c) below). And the small peak in  $\phi_3$  around  $V \sim 0.9$  in Fig. 2 (c) seems to indicated the spontaneous breaking of an extra  $\mathbb{Z}_2$  rotational symmetry with respect to the centers of a plaquette. However, this is a manifestation of an interesting RG flow path starting from the RK towards the RP fixed point, where along the way the Nambu–Goldstone (NG) fixed point of broken  $U(1)$  symmetry (which contains the further  $\mathbb{Z}_2$  rotational symmetry inside a plaquette) is passed by (see the flow diagram in Fig. 4 (a)). But since this RG flow is triggered by a (dangerously) irrelevant operator ( $\cos(4\pi h)$  – translating from the dimer

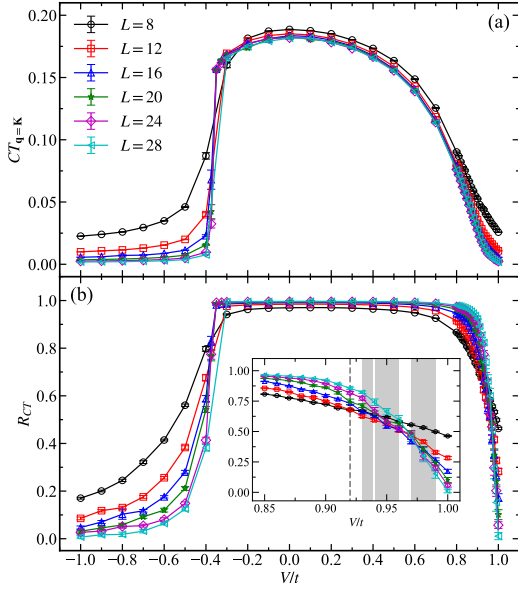


FIG. 3. **Off-diagonal correlation function and correlation ratio.** (a) The static structure factor  $CT_{\mathbf{q}=\mathbf{K}=(\pi,\pi)}$ . The finite value of  $CT$  in the region of  $-0.35(3) < V < 1$  indicates the RP phase. (b) The correlation ratio  $R_{CT}$ . The inset shows the slow drifts in the crossing region of  $R_{CT}$  between consecutive system sizes  $L$ , the crossing regions are denoted by the vertical grey bars, and the drift moves to the RK point at  $V = 1$  in the TDL.

configuration to height variable (see below) – close to the RK point, the finite size scaling of  $\phi_3$  versus  $1/L$ , shown in the inset of Fig. 2 (c), clearly demonstrates that its peak value around  $V \sim 0.9$  eventually extrapolates to 0 as a function of  $L$  in the TDL.

Now that the RP phase does not break the lattice rotation but the translational symmetry. We find the true order parameter of the RP phase shall be computed from the correlation function of the off-diagonal  $t$ -terms of the Hamiltonian,  $CT \equiv \langle t_i t_j \rangle$  where  $i$  is the position of the lower-left site of each plaquette.  $CT$  captures the resonance of the parallel dimer pairs within a plaquette, hence the name RP phase. Since the RP order is invisible from the diagonal probes such as  $\phi_{1,2,3}$  and can only be seen via off-diagonal  $CT$ , it is a new quantum state with *hidden* order which is of interests to Rydberg experiments. The translational symmetry breaking in RP presents itself as  $\mathbf{K} = (\pi, \pi)$  in the static structure factor  $CT_{\mathbf{q}=\mathbf{K}}$  shown in Fig. 3 (a). Besides, its correlation ratio  $R_{CT} = 1 - CT_{\mathbf{q}'}/CT_{\mathbf{q}=\mathbf{K}}$ , where  $CT_{\mathbf{q}'}$  is the average structure factor of the four momenta around  $\mathbf{K}$  point, is shown in Fig. 3 (b).

One sees in the LN phase,  $R_{CT}$  extrapolates to 0 in the TDL and it stays close to 1 in the RP phase, and the discontinuous jump signifies the first order transition at  $V = -0.35(3)$ . The interesting behaviour is close to the RK point, where we observe the crossing of the  $R_{CT}$

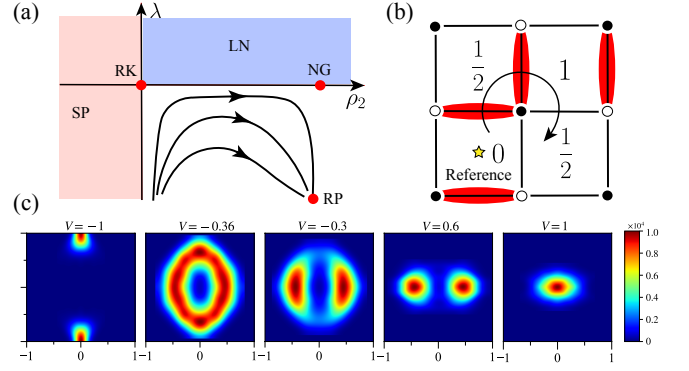


FIG. 4. (a) **Schematic RG flow.** The RK point is at the origin which is a quantum critical point with  $z = 2$ . The coupling constant  $\rho_2$  is proportional to  $V - V_c$  near the RK point.  $\rho_2 > 0$  the flow is towards the RP fixed point with  $\lambda < 0$ , passing the irrelevant Nambu-Goldstone (NG) fixed point, which signifies a further  $\mathbb{Z}_2$  rotational symmetry breaking inside each plaquette, as denoted by the small peak close to  $V \sim 0.9$  in Fig. 2(c). The LN ( $\lambda > 0$ ) and SP ( $\rho_2 < 0$ ) regions are also denoted. (b) **Height representation.** The rule for construct height pattern at a  $2 \times 2$  unit of plaquettes. Here we show the clockwise moving around the  $+2$  "magnetic charge". (c) **Histograms of height variable order parameter**  $\langle \frac{4}{N} \sum_I \cos(2\pi h_I), \frac{4}{N} \sum_I \sin(2\pi h_I) \rangle$  for  $L = 8$  system. The histogram in the LN phase ( $V = -1$ ), at the first order transition ( $V = -0.36$ ), in the RP phase ( $V = -0.3, 0.6$ ) and at the RK point ( $V = 1$ ) are shown. The  $h_I$  in the LN phase is  $\pm 1/4$  and in the RP phase is  $\pm 1/2$  or 0, which correspond to the  $(0, \pm 1)$  and  $(\pm 1, 0)$  and at  $V = -0.36$ , the coexistence of the LN and RP phases at the first order phase transition manifests.

between consecutive  $L$ -s (denoted by the vertical dashed bars in the inset of Fig. 3 (b)), these crossing regions drift towards the RK point at  $V = 1$  as  $L$  increases. This is another signature of the rich RG flow path close to the RK point with the dangerously irrelevant NG operator close by, and although these data demonstrate the RP phase within  $-0.35 < V < 1$ , the relations between different fixed points originated from the RK point in the phase diagram of Fig. 1 (b) clearly deserve further explanations from a field theoretical perspective, as we now turn to.

*Effective action and renormalization-group analysis.*— It is known that the QLM has an effective height field action in the continuum limit [37]. The rule for constructing the height covering is illustrated in Fig. 4 (b). We first choose one plaquette as the reference with zero height, then taking a clockwise (anticlockwise) moving around sites with "magnetic charge"  $+2(-2)$  [6, 51, 52], let the height increase by  $1/2$  when crossing an occupied dimer bond and decrease by  $1/2$  for an empty bond. In this way, dimer coverings  $\{c\}$  can be translated to height coverings  $\{h\}$ , and we further define  $h_I$  as the average of the 4 plaquettes centering the "magnetic charge" site. The representative height covering in the LN, RP and SP phases, are give

in SM [50].

Near the RK point, the QLM can be mapped to a quantum version of the famous six-vertex model [7], which can be described by the following Lifshitz type of Lagrangian [1–4, 7, 9, 53, 54]

$$\mathcal{L} = \frac{1}{2}(\partial_\tau h)^2 + \frac{1}{2}\rho_2(\nabla h)^2 + \frac{\kappa^2}{2}(\nabla^2 h)^2 + \lambda \cos(4\pi h), \quad (2)$$

where  $\rho_2 \propto -(V - V_c)$  with  $V_c = 1$  the RK point. The RG flow diagram of the Lagrangian is shown in Fig. 4 (a). When  $\rho_2 > 0$ , spatial derivative of the height field  $h$  is suppressed, this favours a spatial homogenous  $h_I$ , which is indeed the case in the RP phase (see Fig. S1 (b) in SM [50]). When  $\rho_2 < 0$ ,  $\nabla h$  jumps immediately to its cutoff value, which corresponds to the SP phase in Fig. S1 (c) in SM [50]. The height variable is periodic with the identification  $h = h + 1$ . The  $\lambda \cos(4\pi h)$  term therefore breaks the symmetry from  $U(1)$  to  $\mathbb{Z}_2$ , with  $\lambda < 0$  and the  $\lambda > 0$  favors the RP and LN phases, respectively. The RK point, located at  $\rho_2 = \lambda = 0$ , is a quantum critical point with dynamical critical exponents  $z = 2$ , at which the action is invariant under the scaling symmetry  $\tau \rightarrow l^2\tau$  and  $\mathbf{x} \rightarrow l\mathbf{x}$  and the operator  $\cos(4\pi h)$  is irrelevant, indicating an emergent  $U(1)$  symmetry [5, 7].

We calculate the histogram of the height variable  $\langle \frac{4}{N} \sum_I \cos(2\pi h_I), \frac{4}{N} \sum_I \sin(2\pi h_I) \rangle$ , i.e., average over the lattice, for a  $L = 8$  system, which are shown in Fig. 4 (c). In the LN phase, the order parameter is  $(0, \pm 1)$  with  $h_I = \pm 1/4$ , while that is  $(\pm 1, 0)$  in the RP phase with  $h_I = \pm 1/2$  or 0. At  $V = -0.36$ , the coexistence of the LN and RP phases at the first order phase transition manifests. From the histogram, it is clear that as we approach the RK point, the  $\mathbb{Z}_2$  symmetry gets enhanced to  $U(1)$ , although it is still clear there is a  $\mathbb{Z}_2$  anisotropy at  $V = 1$  in the finite size histogram in Fig. 4 (c), consistent with our data in Fig. 2 (c) and Fig. 3 (b). One might wonder whether this anisotropy correspond to a new phase and our RG flow of Eq. (2), shown schematically in Fig. 4 (a) and date of  $|\frac{4}{N} \sum_I \sin(2\pi h_I)|$  in Fig. S2 in SM, show it is a finite size effect.

The Lagrangian Eq. (2) with positive  $\rho_2$  and  $\lambda = 0$  is precisely the Nambu-Goldstone (NG) Lagrangian that describes the spontaneous symmetry breaking phase of  $U(1)$  symmetry [55–57]. When  $\lambda \neq 0$ , the NG fixed point is unstable under RG flow. At a fixed coupling, the QLM with increasing lattice size can be viewed as an RG flow. Near the RK point, the  $\lambda \cos(4\pi h)$  term is irrelevant, so that the RG flow lingers around the  $\lambda$  close to zero region (in particular, near the NG fixed point) for a very long RG time. This means that a finite-sized QLM will likely to be describe by Eq. (2) with small  $|\lambda|$ . Notice the energy difference between the minimum and the maximum of the  $\lambda \cos(4\pi h)$  is proportional to  $|\lambda|$ . When  $|\lambda|$  is small (and  $\lambda < 0$ ), quantum fluctuations can easily drive vacuum from the RP phase with  $h = \pm 1/2$

or 0 to other values. This explains the non-vanishing  $\phi_3$  at  $V \sim 0.9$  in Fig. 2 (c), the drift of the crossing point in Fig. 3 (b) and the anisotropy of histogram in Fig. 4 (c) at  $V = 1$  in finite size data. Similarly, the expectation value of  $|\frac{4}{N} \sum_I \sin(2\pi h_I)|$ , which is shown in Fig. S2, shows a mild peak in the region of  $0.9 < V < 1$ . A similar RG flow with crossover behaviour was observed in three dimensional classical clock model [58] or in the deconfined quantum critical point where a dangerously irrelevant second length scale is found to mask the still unsettled fixed point [48, 49, 59–62].

The above mentioned RG structure replies on the fact that the operator  $\cos(4\pi h)$  being irrelevant at the RK point. The scaling dimension of  $\cos(4\pi h)$  is related to the “Luttinger parameter”  $\kappa$ . Different with the QDM case ( $\kappa = 2\pi$ ) which can be mapped to the free fermion [2, 3], in the case of QLM, there are in total six possible dimer configurations at each site, which are can be mapped to the six types of vertices of the famous six-vertex model [63]. All correlation functions on the RK vacuum is equivalent to six-vertex model with all six types of vertices appear at equal probability (which are usually called the ice point, referring to the ice rule of water ice by Pauling [64]). It has been known that six-vertex model can be describe as free compact boson models in two dimensions [53]:  $\langle vac | \mathcal{O}[h(x_1)] \dots \mathcal{O}[h(x_n)] | vac \rangle = \frac{1}{\mathcal{Z}} \int [\mathcal{D}h] \mathcal{O}[h(x_1)] \dots \mathcal{O}[h(x_n)] e^{-\kappa \int dx^2 (\nabla h)^2}$ . Here  $\kappa = 2\pi r^2$ , with  $r$  being the radius of the compact boson in the convention of Ref. [65]. At the ice point, one gets  $\kappa = \pi/3$  [53]. The 2d quantum version of this type of model, was derived in Ref. [7] and leads to Eq. (2). The conformal field theory analysis of the free compact boson tells us that the scaling dimension of  $\cos(2\pi n h)$  (and  $\sin(2\pi n h)$ ) is  $\Delta_n = \frac{n^2 \pi}{2\kappa} = \frac{3n^2}{2}$  [66], clearly  $\Delta[\cos(4\pi h)] = 6$ , which is irrelevant.

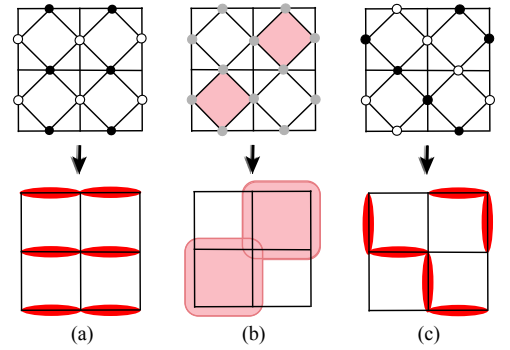


FIG. 5. **Mapping of checkerboard lattice Rydberg atom array to QLM on square lattice.** The correspondences between the Rydberg atom configuration and the (a) LN phase, (b) the RP phase, and (c) the SP of QLM model are demonstrated. The solid (hollow) circle represents the presence (absence) of a Rydberg atom on the bonds of the checkerboard lattice, and the grey circle in (b) donates the resonating of the Rydberg atoms in each tetrahedron.

*Experimental proposal and Discussion.*— The QLM on square lattice can be realized in the Rydberg arrays experiments, which have recently been utilized to probe topological order in QDMs [35, 36]. The effective Hamiltonian of Rydberg arrays is [27, 28]:  $H_R = h \sum_i \sigma_i^x - \mu \sum_i n_i + V \sum_{i>j} \frac{n_i n_j}{|i-j|^6}$ , where  $i$  and  $j$  are the site labels,  $n_i = 0, 1$  is the density operator to probe the ground state or Rydberg state, respectively, and  $\sigma^x$  is the tunneling term to connect the two states. If we only consider the nearest-neighbour (NN) interactions, and the NN runs over the bonds of the 2d checkerboard lattice [39] in Fig. 5. Under the competing between the Rydberg blockade (favoring one particle in Rydberg radius) and chemical potential (inducing more occupied particles), the Rydberg atom configurations will obey the "ice rule" in certain parameter region— every state with exactly two occupied and two empty sites per tetrahedron (cross linked plaquette) [64], i.e., there are two particles in the Rydberg radius. The kind of local constraint has been realized both in experiment [36] and numeric [30].

In the  $h \ll V$  case, any excitation breaks the "ice rule" will lead a huge energy cost at the scale of  $V$ . Therefore, the quantum fluctuations within the "ice rule" becomes the low energy excitations, that is the 4th order term of the  $h$ , i.e.,  $h^4(\sigma_i^+ \sigma_j^- \sigma_k^+ \sigma_l^- + \sigma_i^- \sigma_j^+ \sigma_k^- \sigma_l^+)$ , where the  $i, j, k, l$  are the sites labeled in a plaquette. Thus, the low energy effective model in this case is the QLM in Eq. (1). In this way, the LN, RP and SP states and their interesting phase transitions, the *hidden* nature of the RP as a new quantum state of matter, and the intricate RG flow of with marginal operator in the effective height action, can all be investigated in the Rydberg atom experiments.

*Acknowledgements*—We thank Fabien Alet for valuable discussions on the phase diagrams of QDM and QLM over the years. XXR, ZY and ZYM acknowledge support from the Research Grants Council of Hong Kong SAR of China (Grant Nos. 17303019, 17301420, 17301721, AoE/P-701/20, 17309822 and A-HKU703/22) and the Seed Funding "Quantum-Inspired explainable-AI" at the HKU-TCL Joint Research Centre for Artificial Intelligence. YQ acknowledges support from the the National Natural Science Foundation of China (Grant Nos. 11874115 and 12174068). JR is supported by Huawei Young Talents Program at IHES. YCW acknowledges the support of Beihang Hangzhou Innovation Institute Yuhang and the support from the National Natural Science Foundation of China (Grant Nos. 11804383 and 11975024). We thank HPC2021 system under the Information Technology Services and the Blackbody HPC system at the Department of Physics, the University of Hong Kong for their technical support and generous allocation of CPU time.

- 
- \* zhengyan@hku.hk  
† zymeng@hku.hk
- [1] M. E. Fisher, Phys. Rev. **124**, 1664 (1961).
  - [2] P. Kasteleyn, Physica **27**, 1209 (1961).
  - [3] H. N. Temperley and M. E. Fisher, Philosophical Magazine **6**, 1061 (1961).
  - [4] M. E. Fisher and J. Stephenson, Phys. Rev. **132**, 1411 (1963).
  - [5] S. A. Kivelson, D. S. Rokhsar, and J. P. Sethna, Phys. Rev. B **35**, 8865 (1987).
  - [6] D. A. Huse, W. Krauth, R. Moessner, and S. L. Sondhi, Phys. Rev. Lett. **91**, 167004 (2003).
  - [7] E. Ardonne, P. Fendley, and E. Fradkin, Annals of Physics **310**, 493 (2004).
  - [8] F. Alet, J. L. Jacobsen, G. Misguich, V. Pasquier, F. Mila, and M. Troyer, Phys. Rev. Lett. **94**, 235702 (2005).
  - [9] F. Alet, Y. Ikhlef, J. L. Jacobsen, G. Misguich, and V. Pasquier, Phys. Rev. E **74**, 041124 (2006).
  - [10] R. Moessner and S. L. Sondhi, Phys. Rev. Lett. **86**, 1881 (2001).
  - [11] R. Moessner, S. L. Sondhi, and P. Chandra, Phys. Rev. B **64**, 144416 (2001).
  - [12] R. Moessner and S. L. Sondhi, Phys. Rev. B **63**, 224401 (2001).
  - [13] E. Fradkin, D. A. Huse, R. Moessner, V. Oganesyan, and S. L. Sondhi, Phys. Rev. B **69**, 224415 (2004).
  - [14] R. Moessner and K. S. Raman, "Quantum dimer models," in *Introduction to Frustrated Magnetism: Materials, Experiments, Theory*, edited by C. Lacroix, P. Mendels, and F. Mila (Springer Berlin Heidelberg, Berlin, Heidelberg, 2011) pp. 437–479.
  - [15] B. Dabholkar, G. J. Sreejith, and F. Alet, Phys. Rev. B **106**, 205121 (2022).
  - [16] D. Charrier and F. Alet, Phys. Rev. B **82**, 014429 (2010).
  - [17] D. Charrier, F. Alet, and P. Pujol, Phys. Rev. Lett. **101**, 167205 (2008).
  - [18] P. W. Anderson, science **235**, 1196 (1987).
  - [19] D. S. Rokhsar and S. A. Kivelson, Phys. Rev. Lett. **61**, 2376 (1988).
  - [20] N. Read and S. Sachdev, Phys. Rev. Lett. **66**, 1773 (1991).
  - [21] X. G. Wen, Phys. Rev. B **44**, 2664 (1991).
  - [22] R. A. Jalabert and S. Sachdev, Phys. Rev. B **44**, 686 (1991).
  - [23] D. A. Ivanov, Phys. Rev. B **70**, 094430 (2004).
  - [24] A. Ralko, M. Ferrero, F. Becca, D. Ivanov, and F. Mila, Phys. Rev. B **71**, 224109 (2005).
  - [25] A. Ralko, M. Ferrero, F. Becca, D. Ivanov, and F. Mila, Phys. Rev. B **74**, 134301 (2006).
  - [26] A. Ralko, M. Ferrero, F. Becca, D. Ivanov, and F. Mila, Phys. Rev. B **76**, 140404 (2007).
  - [27] M. Saffman, T. G. Walker, and K. Mølmer, Rev. Mod. Phys. **82**, 2313 (2010).
  - [28] A. Browaeys and T. Lahaye, Nature Physics **16**, 132 (2020).
  - [29] H. Bernien, S. Schwartz, A. Keesling, H. Levine, A. Omran, H. Pichler, S. Choi, A. S. Zibrov, M. Endres, M. Greiner, V. Vuletić, and M. D. Lukin, Nature **551**, 579 (2017).
  - [30] R. Samajdar, W. W. Ho, H. Pichler, M. D. Lukin,



- and S. Sachdev, Proc. Nat. Acad. Sci. **118**, e2015785118 (2021).
- [31] R. Verresen, M. D. Lukin, and A. Vishwanath, Phys. Rev. X **11**, 031005 (2021).
- [32] Z. Yan, R. Samajdar, Y.-C. Wang, S. Sachdev, and Z. Y. Meng, Nature Communications **13**, 5799 (2022).
- [33] P. Scholl, M. Schuler, H. J. Williams, A. A. Eberharter, D. Barredo, K.-N. Schymik, V. Lienhard, L.-P. Henry, T. C. Lang, T. Lahaye, A. M. Läuchli, and A. Browaeys, Nature **595**, 233 (2021).
- [34] S. Ebadi, T. T. Wang, H. Levine, A. Keesling, G. Semeghini, A. Omran, D. Bluvstein, R. Samajdar, H. Pichler, W. W. Ho, S. Choi, S. Sachdev, M. Greiner, V. Vuletić, and M. D. Lukin, Nature **595**, 227 (2021).
- [35] K. J. Satzinger, Y. J. Liu, A. Smith, C. Knapp, M. Newman, C. Jones, Z. Chen, C. Quintana, X. Mi, A. Dunsworth, C. Gidney, I. Aleiner, F. Arute, K. Arya, J. Atalaya, R. Babbush, J. C. Bardin, R. Barends, J. Basso, A. Bengtsson, A. Bilmes, M. Broughton, B. B. Buckley, D. A. Buell, B. Burkett, N. Bushnell, B. Chiaro, R. Collins, W. Courtney, S. Demura, A. R. Derk, D. Eppens, C. Erickson, L. Faoro, E. Farhi, A. G. Fowler, B. Foxen, M. Giustina, A. Greene, J. A. Gross, M. P. Harrigan, S. D. Harrington, J. Hilton, S. Hong, T. Huang, W. J. Huggins, L. B. Ioffe, S. V. Isakov, E. Jeffrey, Z. Jiang, D. Kafri, K. Kechedzhi, T. Khattar, S. Kim, P. V. Klimov, A. N. Korotkov, F. Kostritsa, D. Landhuis, P. Laptev, A. Locharla, E. Lucero, O. Martin, J. R. McClean, M. McEwen, K. C. Miao, M. Mohseni, S. Montazeri, W. Mruczkiewicz, J. Mutus, O. Naaman, M. Neeley, C. Neill, M. Y. Niu, T. E. O'Brien, A. Opremcak, B. Pató, A. Petukhov, N. C. Rubin, D. Sank, V. Shvarts, D. Strain, M. Szalay, B. Villalonga, T. C. White, Z. Yao, P. Yeh, J. Yoo, A. Zalcman, H. Neven, S. Boixo, A. Megrant, Y. Chen, J. Kelly, V. Smelyanskiy, A. Kitaev, M. Knap, F. Pollmann, and P. Roushan, Science **374**, 1237 (2021).
- [36] G. Semeghini, H. Levine, A. Keesling, S. Ebadi, T. T. Wang, D. Bluvstein, R. Verresen, H. Pichler, M. Kalinowski, R. Samajdar, A. Omran, S. Sachdev, A. Vishwanath, M. Greiner, V. Vuletić, and M. D. Lukin, Science **374**, 1242 (2021).
- [37] C. L. Henley, Journal of Statistical Physics **89**, 483 (1997).
- [38] A. M. Läuchli, S. Capponi, and F. F. Assaad, Journal of Statistical Mechanics: Theory and Experiment **2008**, P01010 (2008).
- [39] N. Shannon, G. Misguich, and K. Penc, Phys. Rev. B **69**, 220403 (2004).
- [40] K. Roychowdhury, S. Bhattacharjee, and F. Pollmann, Phys. Rev. B **92**, 075141 (2015).
- [41] X. Plat, F. Alet, S. Capponi, and K. Totsuka, Phys. Rev. B **92**, 174402 (2015).
- [42] Z. Yan, Y. Wu, C. Liu, O. F. Syljuåsen, J. Lou, and Y. Chen, Phys. Rev. B **99**, 165135 (2019).
- [43] Z. Yan, Y.-C. Wang, N. Ma, Y. Qi, and Z. Y. Meng, npj Quantum Mater. **6**, 39 (2021).
- [44] Z. Yan, Phys. Rev. B **105**, 184432 (2022).
- [45] Z. Yan, Z. Zhou, O. F. Syljuåsen, J. Zhang, T. Yuan, J. Lou, and Y. Chen, Phys. Rev. B **103**, 094421 (2021).
- [46] Z. Yan, Z. Y. Meng, D. A. Huse, and A. Chan, Phys. Rev. B **106**, L041115 (2022).
- [47] Z. Yan, X. Ran, Y.-C. Wang, R. Samajdar, J. Rong, S. Sachdev, Y. Qi, and Z. Y. Meng, arXiv e-prints , arXiv:2205.04472 (2022), arXiv:2205.04472 [cond-mat.str-el].
- [48] T. Senthil, L. Balents, S. Sachdev, A. Vishwanath, and M. P. A. Fisher, Phys. Rev. B **70**, 144407 (2004).
- [49] H. Shao, W. Guo, and A. W. Sandvik, Science **352**, 213 (2016).
- [50] Implementation of the sweeping cluster QMC for the two-dimers-per-site constraint, the translation from the dimer covering to the height covering and the representative height coverings in the LN, RP and SP phases and the finite size scaling of the height order parameters are presented in the Supplemental Material.
- [51] N. Wilkins and S. Powell, Phys. Rev. B **99**, 144403 (2019).
- [52] N. Wilkins and S. Powell, Phys. Rev. B **102**, 174431 (2020).
- [53] P. Di Francesco, H. Saleur, and J.-B. Zuber, Journal of statistical physics **49**, 57 (1987).
- [54] E. Fradkin, D. A. Huse, R. Moessner, V. Oganesyan, and S. L. Sondhi, Phys. Rev. B **69**, 224415 (2004).
- [55] Y. Nambu, Phys. Rev. **117**, 648 (1960).
- [56] J. Goldstone, Il Nuovo Cimento (1955-1965) **19**, 154 (1961).
- [57] J. Goldstone, A. Salam, and S. Weinberg, Phys. Rev. **127**, 965 (1962).
- [58] H. Shao, W. Guo, and A. W. Sandvik, Phys. Rev. Lett. **124**, 080602 (2020).
- [59] A. Nahum, J. T. Chalker, P. Serna, M. Ortuño, and A. M. Somoza, Phys. Rev. X **5**, 041048 (2015).
- [60] J. Zhao, Y.-C. Wang, Z. Yan, M. Cheng, and Z. Y. Meng, Phys. Rev. Lett. **128**, 010601 (2022).
- [61] Y.-C. Wang, N. Ma, M. Cheng, and Z. Y. Meng, SciPost Phys. **13**, 123 (2022).
- [62] Z. H. Liu, W. Jiang, B.-B. Chen, J. Rong, M. Cheng, K. Sun, Z. Y. Meng, and F. F. Assaad, arXiv e-prints , arXiv:2212.11821 (2022), arXiv:2212.11821 [cond-mat.str-el].
- [63] J. d. Gier, in *Polygons, Polyominoes and Polycubes* (Springer, 2009) pp. 317–346.
- [64] L. Pauling, J. Am. Chem. Soc. **57**, 2680 (1935).
- [65] P. Ginsparg, Nuclear Physics B **295**, 153 (1988).
- [66] P. H. Ginsparg, in *Les Houches Summer School in Theoretical Physics: Fields, Strings, Critical Phenomena* (1988) arXiv:hep-th/9108028.
- [67] K. Roychowdhury, S. Bhattacharjee, and F. Pollmann, Phys. Rev. B **92**, 075141 (2015).
- [68] F. Vernay, A. Ralko, F. Becca, and F. Mila, Phys. Rev. B **74**, 054402 (2006).
- [69] O. F. Syljuåsen, Phys. Rev. B **71**, 020401 (2005).
- [70] O. F. Syljuåsen, Phys. Rev. B **73**, 245105 (2006).
- [71] D. Banerjee, F.-J. Jiang, P. Widmer, and U.-J. Wiese, Journal of Statistical Mechanics: Theory and Experiment **2013**, P12010 (2013).
- [72] D. Banerjee, M. Bögli, C. P. Hofmann, F.-J. Jiang, P. Widmer, and U.-J. Wiese, Phys. Rev. B **90**, 245143 (2014).
- [73] D. Banerjee, M. Bögli, C. P. Hofmann, F.-J. Jiang, P. Widmer, and U.-J. Wiese, Phys. Rev. B **94**, 115120 (2016).
- [74] O. F. Syljuåsen, Int. J. Mod. Phys. B **19**, 1973 (2005).
- [75] O. F. Syljuåsen and A. W. Sandvik, Phys. Rev. E **66**, 046701 (2002).
- [76] F. Alet, S. Wessel, and M. Troyer, Phys. Rev. E **71**, 036706 (2005).

## Supplemental Material for “Fully packed quantum loop model on the square lattice: phase diagram and application for Rydberg atoms”

In this Supplemental Material, we firstly give detailed discussion about the height patterns in the LN, RP, and SP states to show their correspondence with the Lagrangian given in Eq. (2) in the main text, as well as its relations between the height order parameter  $|\frac{4}{N} \sum_I \sin(2\pi h_I)|$ , the histogram demonstrated in Fig. 4 (c), and the order parameters shown in Fig. 2. Next, the sweeping cluster QMC method is introduced including several details of our simulations. Finally, the scaling of the height order parameter  $|\frac{4}{N} \sum_I \sin(2\pi h_I)|$  and  $|\frac{4}{N} \sum_I \cos(2\pi h_I)|$  are displayed to show the manifestation of the emergent  $U(1)$  symmetry at the RK point.

### HEIGHT PATTERNS AND ORDER PARAMETER

According to the height pattern construction rule illustrated in Fig. 4 (b), here we show the height patterns for  $V = -1$  (LN phase),  $V = 0.3$  (RP phase), and  $V > 1$  (SP) as shown in Fig. S1. For the LN and RP phases, we choose one dimer configuration in our QMC simulations for each phase, the distribution of the average height variable  $h_I$  consist with the histogram indicated in Fig. 4 (c), where  $h_I = \pm 1/4$  in LN phase and  $h_I = \pm 1/2$  or 0 in RP phase. For the SP, we give an ideal dimer configuration to show the height pattern with the Lagrangian parameter  $\rho_2 < 0$ . Since the  $\nabla h$  is a finite value and  $h$  is periodic with respect to  $L$ . We shall construct the height pattern in a finite lattice with caution. When the reference height is fixed with 0 in the first plaquette, we first give the height variables of the diagonal plaquettes, then determine its value of the upper (lower) triangular plaquettes according to the upper left (lower right) height variable of the diagonal plaquettes. In this way, we can find the along the diagonal of our lattice  $|\nabla h| = 1$  and the period of the height variable is  $L/2$ .

The height order parameter  $|\frac{4}{N} \sum_I \sin(2\pi h_I)|$  for different system sizes is shown in Fig. S2, which indicates the same small peak in the region of  $0.9 < V < 1$  as the order parameters in Fig. 2 (c).  $\frac{4}{N} \sum_I \sin(2\pi h_I)$  is the  $y$  component of the histograms illustrated in Fig. 4 (c), which corresponds to  $\pm 1$  in LN phase and 0 in RP phase. The mild peaks of the order parameter exhibit the dangerously irrelevant  $\mathbb{Z}_2$  instability at  $V \sim 0.9$  close to the RK point and will eventually vanish at the thermodynamic limit.

### SWEEPING CLUSTER QUANTUM MONTE CARLO WITH TWO DIMERS PER SITE

The sweeping cluster QMC approach employed in this work is a new method developed by us, which works well in constrained quantum lattice models [42–44]. Prior to sweeping cluster QMC, to solve the QDM or QLM types of

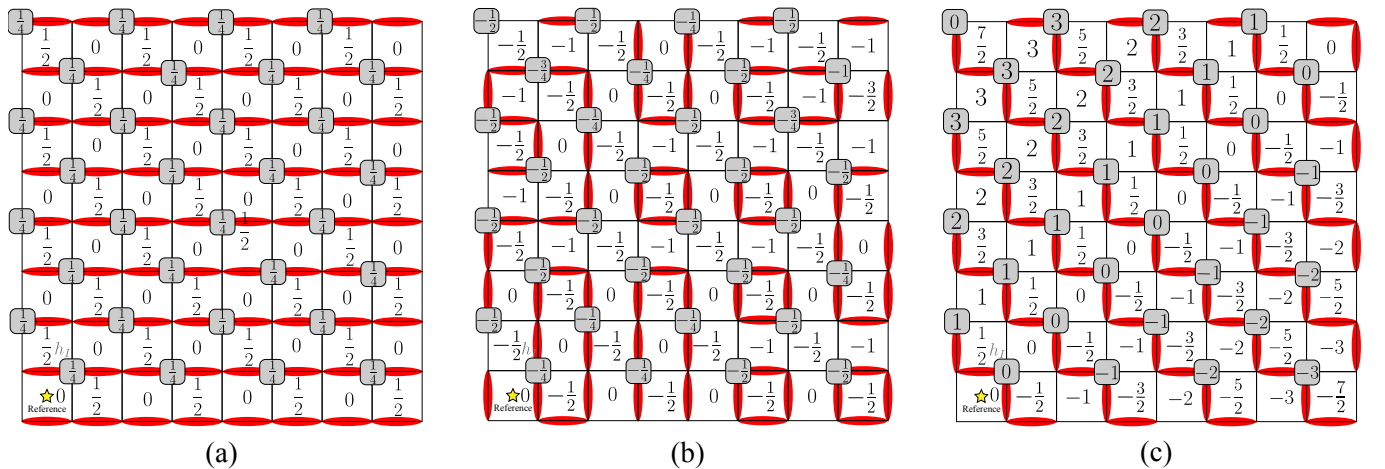


FIG. S1. Height pattern for dimer coverings when (a)  $V = -1$ , (b)  $V = 0.3$ , and (c)  $V > 1$  on a  $8 \times 8$  lattice, corresponding to the LN, RP, and SP states discussed in the main text. The height value in each plaquette is given by the rule shown in Fig. 4 (b), which shows the clockwise moving around the +2 "magnetic charge". The values in the grey rectangle are the average height  $h_I$  of the  $2 \times 2$  unit. The values of the height variable in the LN, RP and SP states are consistent with the RG analyze. In the SP, the height variable is periodic with respect to  $L$ .

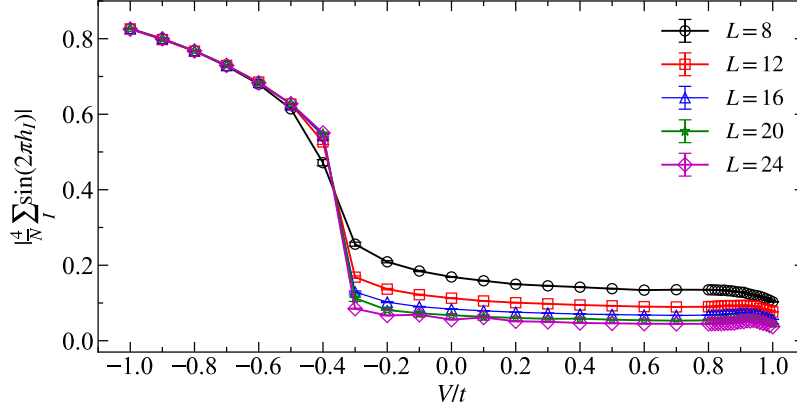


FIG. S2. The height order parameter  $|\frac{4}{N} \sum_i \sin(2\pi h_I)|$  for different system sizes, which shows the same behaviour as the order parameters in Fig. 2. The mild peaks in the region of  $0.9 < V < 1$  are the finite size effect which result in the anisotropy of the histogram shown in Fig. 4 (c).

constrained models, one had to rely on either exact diagonalization of small systems, or variational approaches such as DMRG that suffer from finite-size effects on the cylindrical geometry [67], or the projector Monte Carlo approaches, which include the Green's function [23–26, 41, 68] and diffusion Monte Carlo schemes [69, 70], or sampling directly in height space and throwing away the unconstrained configurations [71–73]. These projector Monte Carlo methods obey the geometric constraints but are not efficient away from the RK point [74] and only work at  $T = 0$ . Furthermore, there does not exist any cluster update for the projector methods. On the contrary, the sweeping cluster algorithm is based on the world-line Monte Carlo scheme [8, 75, 76] to sweep and update layer by layer along the imaginary time direction so that the local constraints (gauge field) are recorded by update lines. In this way, all the samplings are done in the restricted Hilbert space and it contains the cluster update scheme for constrained systems [44] and works at all temperatures. Proper finite size scaling analysis can then be carried out to explore phase transitions and critical phenomena.

We set the initial state as one of the two LN patterns with the same probability for satisfy the two dimer per site constraint in our QMC simulation. The random initialization has no influence on the QMC results[47]. We simulate  $L \times L$  square lattices with system sizes  $L = 8, 12, 16, 20, 24, 28$  with the inverse temperature set to  $\beta = 2L$  and  $10^5$  Monte Carlo samplings used to obtain average values of the observables in all calculations.